Oxid Met (2009) 71:173–186
DOI 10.1007/s11085-008-9134-x

ORIGINAL PAPER

Effect of Chromium Content on the Oxidation Behaviour of Ferritic Steels for Applications in Steam Atmospheres at High Temperatures

L. Sánchez · M. P. Hierro · F. J. Pérez

Received: 11 March 2008 / Revised: 28 November 2008 / Published online: 14 January 2009

Abstract Environments containing water vapour are common in many industrial processes, such as power generation systems. Hence, long-term oxidation (1000 h) of P-91 and AISI 430 was studied at 650 and 800 °C, in 100% H_2O atmosphere. The oxidation resistance of the AISI 430 is better than that of the P-91, due to the formation of protective phases on the surface. At 650 °C, a scale composed of Fe_3O_4, Fe_2O_3 and $(Fe,Cr)_3O_4$ is formed on P-91, although at 800 °C the scale is mainly composed of Fe_3O_4 and $(Fe,Cr)_3O_4$. On the other hand, on AISI 430 the scale is composed mainly of $(Fe,Cr)_2O_3$ at 650 °C, and at 800 °C a layer of Cr_2O_3 is formed and remains owing to the higher diffusion rate of Cr at this temperature than at 650 °C, the latter of which compensates the Cr depletion by the degradation of the chromia scale.

Keywords Steam oxidation · Ferritic-martensitic steel · Ferritic stainless steel

Introduction

One of the most important goals in materials that operate at high temperatures is their oxidation resistance. It is well known that ferritic stainless steels have very

L. Sánchez · M. P. Hierro · F. J. Pérez
Grupo Investigación de Ingeniería de Superficies y Materiales Nanoestructurados, Facultad de Ciencias Químicas, Universidad Complutense de Madrid, n° 910627, Avenida Complutense, s/n, 28040 Madrid, Spain

L. Sánchez (✉)
Departamento Ciencia de Materiales e Ingeniería Metalúrgica, Facultad de Ciencias Químicas, Universidad Complutense de Madrid, Avenida Complutense, s/n, 28040 Madrid, Spain
e-mail: lsanche@quim.ucm.es

good properties against corrosion and oxidation, since these steels form a Cr_2O_3 scale under dry atmospheres [1]. On the other hand, the behaviour of 9% Cr ferritic-martensitic steels in dry air at high temperatures is acceptable, due to the formation of a protective scale [2], which composition is dependent of the oxidation temperature. In this way, between 400 and 600 °C the oxide layer is composed mainly of a mixture of FeO, Fe_2O_3 and Cr_2O_3, and at temperatures higher than 600 °C, the scale principally consist of Cr_2O_3 [3, 4]. But operation atmospheres composed of water vapour or mixtures of steam and oxygen are much more corrosive environments than dry air [1, 5, 6], subsequently the scales that grow, are composed of other less protective oxides than Fe_2O_3 or Cr_2O_3.

The oxidation behaviour of Fe–Cr alloys in steam atmospheres has been studied since the sixties [7, 8] and nowadays this issue is still a focus of study, specially for the steam and solid oxide fuel cell power plants components [9, 10]. Corrosion rate is influenced by more than just the type of material or their alloying elements. In the steam corrosion several factors play an important role in the oxidation rate, such as the environmental partial pressure of H_2O [5, 6], the flow rate of the water vapour [4, 11], the superficial roughness of the material [6], the grain size of the alloy [12], or the temperature of exposure [13, 14].

In this way, the temperature is one of the most important parameters in steam oxidation. Normally, when temperature is raised the oxidation rate increases, although in the steam oxidation of Fe–Cr alloys an anomalous temperature dependence can occur due to the stability of protective phases in presence of water vapour and the subsequent distribution of chromium in the oxide scale [14, 15].

The oxidation resistance is related to the chromium content at the material/oxide scale interface. If this chromium content depletes too much during oxidation, non-protective oxides appear by cracking or spalling of the protective scale. On the other hand, some authors suggest that the stability of these chromium oxides are conditioned to the evaporation of chromium by formation of a volatile species [5, 11, 15, 16]. In 9% Cr ferritic-martensitic steels, the oxidation mechanism strongly differs in steam atmospheres from dry air [13]. In this case, the possible anomalous temperature dependence is related to the difference in the distribution of chromium in the inner part of the oxide scale [14]. In the behaviour against the steam oxidation of Fe–Cr alloys, the faster diffusion of chromium with increasing temperature plays an important role in the observed anomalous temperature dependence [1, 14, 17].

In the present work, two different steels, AISI 430 ferritic stainless steel and P-91 martensitic steel have been tested under steam oxidation conditions at two different temperatures, 650 and 800 °C. The main goal of this study was to determine the influence of two critical parameters in steam oxidation. The first is the influence of the chromium content and the second is the influence of the temperature of steam oxidation, associated with the different diffusion rate of chromium.

Experimental Procedure

Target Materials

The tested materials were P-91 ferritic-martensitic steel and AISI 430 ferritic stainless steel. Before oxidation test, the samples (20 × 10 × 2 mm) were ground up to 600-grit SiC paper and then degreased in acetone in ultrasonic bath for 5 min. The chemical compositions obtained by EDX microanalysis of the materials are summarized in Table 1.

Steam Oxidation Test

The P-91 and AISI 430 specimens were tested in steam oxidation, which was carried out in a tubular furnace with a steam atmosphere of 100% of H_2O up to 1000 h at two different temperatures, 650 °C and 800 °C. The steam was generated in other tubular furnace, which is connected with the furnace were the samples are located. The steam passes trough the samples furnace and then is condensed and circulated again. The samples were removed from the tubular furnace at fixed intervals and weighed obtaining the mass change data with the increasing of the oxidation time.

Thermodynamic Approximation

Thermodynamic calculations using Thermo-Calc software [18] were carried out to obtain the solid phases that are stable in the thermodynamic equilibrium, at the conditions used in the steam oxidation.

Characterization Techniques

The specimens after oxidation test were characterized and analyzed by optical microscopy, OM, (LEICA, DM IRM), scanning electron microscopy SEM (JEOL, JM-6400), with energy dispersive X-ray spectroscopy (EDX) performing a standardless analyses. The phase composition of the crystalline corrosion compounds was identified by X-ray diffraction (XRD) using a PHILIPS X′PERT equipped with normal incidence and a PHILIPS X′PERT MPD diffractometer with grazing incidence (XRD-GI), using monochromatic Cu K_α radiation.

Table 1 Chemical composition (weight percent) of P-91 and AISI 430 obtained by EDX analysis

	Fe	Cr	V	Ni	Mo	Mn	Si	Cu	W	C	Other
P-91	Val.	9.20	0.22	0.38	0.90	0.50	0.40	x	x	0.09	Sn, C, N, P, S < 0.2%
AISI 430	Val.	16.21	x	0.18	0.01	0.20	0.40	0.03	x	0.07	

Results

Specimen Mass Change

The experiments of isothermal steam oxidation were carried out at two different temperatures, 650 °C and 800 °C, under atmospheric pressure up to 1000 h and Fig. 1 illustrates the weight change data of the steels during the steam oxidation test, which are used to discuss the oxidation kinetics, for each steel and temperature, the data can be fitted to the relationship $\Delta m = kt^a$ [19] where Δm is the specific weight loss [mg cm^{-2}], t the oxidation time [hours], k and a, constants. At two oxidation temperatures, the behaviour in oxidation of the P-91 steel is worse than that of AISI 430. At 650 °C, the weight change in the AISI 430 is approximately 10 times less than that in the case of the P-91, whereas at 800 °C this difference in the weight change is increased up until more than 60 times less.

On the other hand, in the temperature range of 650–800 °C, these steels have different temperature oxidation dependence. AISI 430 exhibit increasing oxidation rates with decreasing temperature, while in the case of P-91, the oxidation rate is higher when the temperature oxidation is raised up to 800 °C.

Oxide Scale Characterization

Steam Oxidation on P-91

Figures 2 and 3 show the images of the cross sections of P-91 samples after 1000 h of exposure under steam atmosphere at 650 °C (OM image) and 800 °C (SEM image), respectively. In both cases, no scale spallation was observed on the samples

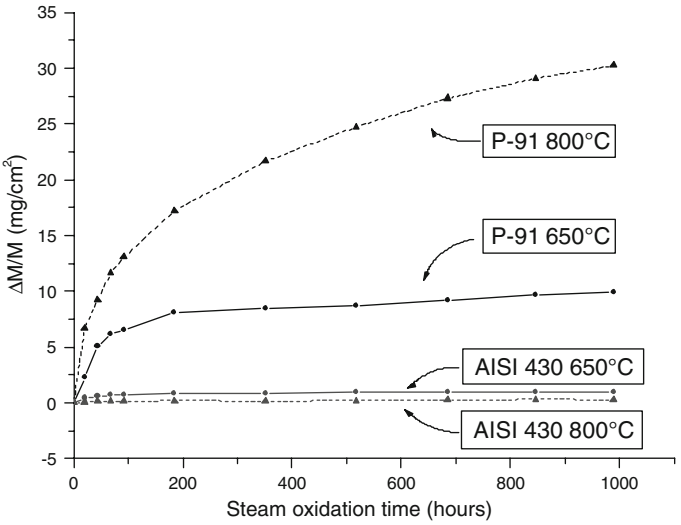

Fig. 1 Weight change of P-91 and AISI 430 steels during steam exposure at 650 °C and 800 °C

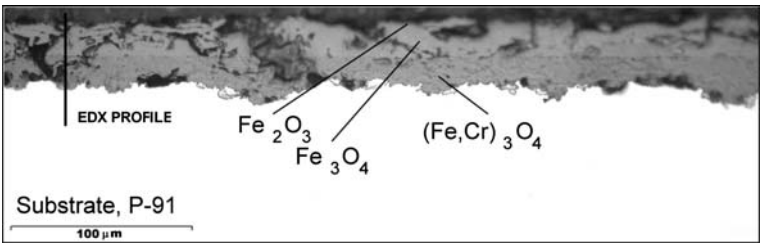

Fig. 2 OM image of P-91 ferritic-martensitic steel after steam oxidation at 650 °C up to 1000 h

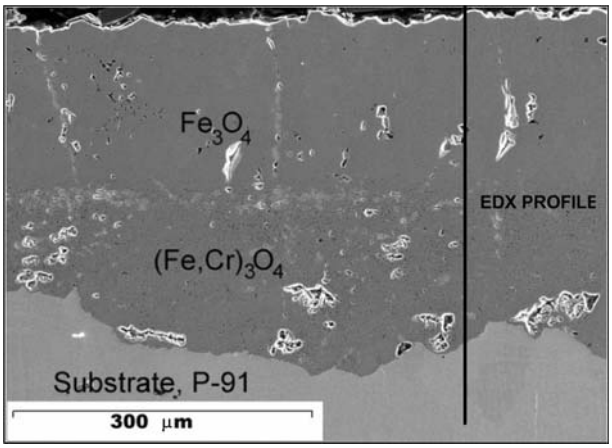

Fig. 3 SEM image of P-91 ferritic-martensitic steel after steam oxidation at 800 °C up to 1000 h

and the microstructure of the oxide scale exhibit a porous and bi-layered structure. In the oxidized sample at 650 °C, the scale thickness is 40–50 μm, whereas when the operation test was 800 °C the scale thickness raised up to 80–100 μm. These results are in agreement with the weight change curves of P-91, since a thicker oxide scale entails a higher mass gain.

The phase composition of the oxide scales growth on P-91 was obtained by means of XRD and is summarized in Table 2. The diffraction results of the scale formed at 650 °C show the presence of hematite (Fe_2O_3) and magnetite (Fe_3O_4). On the other hand, in the XRD of the oxidized P-91 at 800 °C only the magnetite phase has been identified.

With the purpose of obtaining the chemical composition of the oxide scales, the polished cross sections of the specimens were analyzed by EDX. The EDX line scan analyses of the P-91 samples oxidized in 100% vapour atmosphere for 1000 h at 650 °C and 800 °C are given in Fig. 4, which shows that the concentration profiles exhibit a similar tendency at two studied temperatures; the chemical composition of the outer layer of the scale is mainly composed of iron and oxygen, that correspond to iron oxides, whereas the inner layer of the scale is formed of oxides of iron and

Table 2 XRD data of the P-91 after steam oxidation up to 1000 h at 650 °C

XRD results of P-91 after 1000 h in 100% H_2O		
Test Temp. 650 °C Diffraction angle, 2θ	Test Temp. 800 °C Diffraction angle, 2θ	Phase ascribed
24.12		Fe_2O_3
30.10	30.23	Fe_3O_4
33.17		Fe_2O_3
35.39	35.52	Fe_3O_4
40.82		Fe_2O_3
43.05	43.18	Fe_3O_4
49.45		Fe_2O_3
53.43	53.56	Fe_3O_4
54.03		Fe_2O_3
56.97	57.05	Fe_3O_4
62.53	62.74	Fe_3O_4
64.06		Fe_2O_3
71.02	71.15	Fe_3O_4

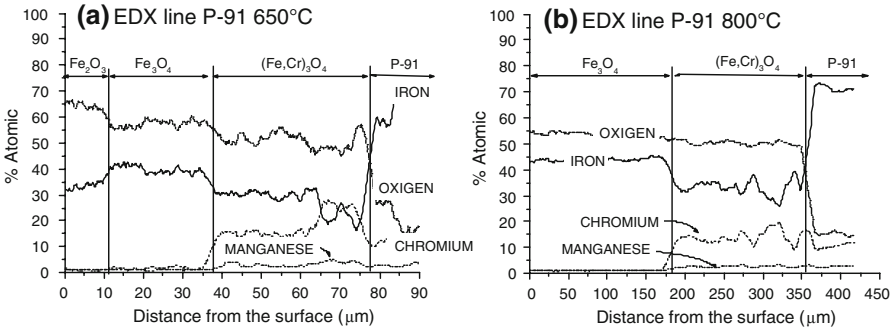

Fig. 4 EDX line scan analysis of ferritic-martensitic steel after steam exposure up to 1000 h at **a** 650 °C and **b** 800 °C

chromium. Finally, no significant amount of manganese in the oxide scales was detected.

As shown the XRD and EDX results, the phase composition of the oxide layers is different at two oxidation temperatures. When oxidation test was carried out at 650 °C, tree different phases are growth on the steel surface. In agreement with EDX analysis, the hematite detected by XRD is placed at the outermost zone and magnetite phase is placed below the hematite. In the EDX analysis, the oxygen concentration in the zone assigned to the magnetite and in the inner area is similar, so the oxide in the inner area must be a M_3O_4 type, which is identified as $(Fe,Cr)_3O_4$ spinel.

When the oxidation is carried out at 800 °C, two phases are only identified in the scale. The outer layer is composed of magnetite phase and the inner region of Fe/Cr

spinel, $(Fe,Cr)_3O_4$, since the EDX analysis reveals that the amount of oxygen in practically the same in the whole of the scale.

Steam Oxidation on AISI 430

As shown the gravimetric curves of Fig. 1, oxidation rate of AISI 430 is lower than that of the P-91. The difference in the behaviour can also be observed in the cross sections of the oxidized samples. Figures 5 and 6 shows the images of the AISI 430 cross sections after 1000 h of steam oxidation, at 650 (OM image) and 800 °C (SEM image), respectively.

In the case of the steam oxidation of the AISI 430 at 650 °C, two different areas can be shown in the scale, the substrate surface is coated by a thin and dark layer and in several areas of the surface, and elongated nodules are grown. On the contrary, when the oxidation temperature is raised up to 800 °C, the surface of the AISI 430 is totally coated of a bi-layered scale. The thickness of the outer layer (light colour) is approximately 2 μm, whereas the thickness of inner area is lower than 1 μm.

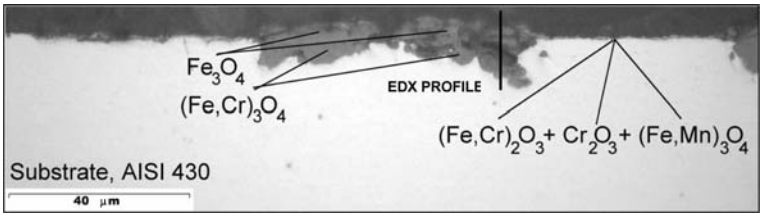

Fig. 5 OM image of AISI 430 ferritic stainless steel after steam oxidation at 650 °C up to 1000 h

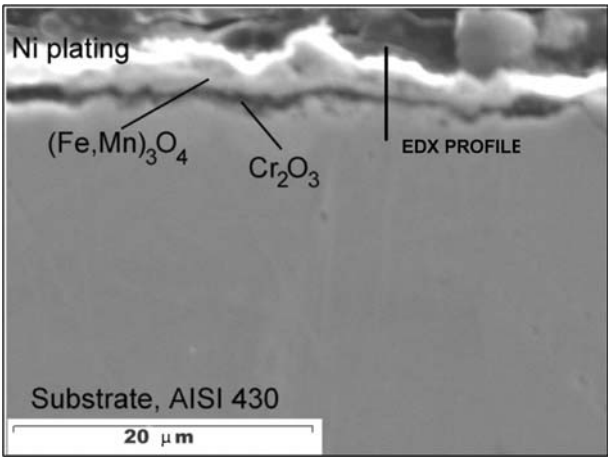

Fig. 6 SEM image of AISI 430 AISI 430 ferritic stainless steel after steam oxidation at 800 °C up to 1000 h

Table 3 XRD data of the P-91 after steam oxidation up to 1000 h at 800 °C

XRD results of AISI 430 after 1000 h in 100% H_2O		
Test Temp. 650 °C Diffraction angle, 2θ	Test Temp. 800 °C Diffraction angle, 2θ	Phase ascribed
24.16		$(Fe,Cr)_2O_3$
	24.40	Cr_2O_3
29.75	29.83	$(Fe,Mn)_3O_4$
30.05		Fe_3O_4
33.23		$(Fe,Cr)_2O_3$
	33.58	Cr_2O_3
34.90	34.96	$(Fe,Mn)_3O_4$
25.65		Fe_3O_4
	36.09	Cr_2O_3
40.94		$(Fe,Cr)_2O_3$
	41.38	Cr_2O_3
	42.63	$(Fe,Mn)_3O_4$
43.07		Fe_3O_4
44.57	44.58	Fe
49.42		$(Fe,Cr)_2O_3$
50.17	50.25	Cr_2O_3
54.10		Fe_3O_4
54.70	54.74	Cr_2O_3
55.91	56.02	$(Fe,Mn)_3O_4$
56.28		$(Fe,Cr)_2O_3$
57.74		Fe_3O_4
61.66	61.78	$(Fe,Mn)_3O_4$
62.57		Fe_3O_4
64.09		$(Fe,Cr)_2O_3$
	63.23	Cr_2O_3
65.15	65.23	Fe
71.95		Fe_3O_4

XRD and XRD-GI analyses were carried out on the oxidized AISI 430. The most representative diffraction peaks are given in Table 3. In the samples oxidized at 650 °C, the more intense diffractions peaks are attributed to the $(Fe,Cr)_3O_4$, $(Fe,Cr)_2O_3$ and iron-α (substrate diffractions), although a slight diffractions are also observed, identifying chromia (Cr_2O_3) and Fe/Mn spinel ($(Fe,Mn)_3O_4$). The diffractions peaks assigned to the Fe/Mn spinel have a slight difference in the diffraction angle with respect to the Fe_3O_4, as shown the experimental results and the published diffraction patterns of these phases (JCPDS 11-0614(Fe_3O_4), 73-1964 ($MnFe_2O_4$) and 75-0035 ($FeMn_2O_4$)). On the contrary, only chromia, Fe/Mn spinel and iron-α are identified when the steam oxidation temperature was 800 °C.

The EDX analyses of the oxidized AISI 430 are shown in Fig. 7. Figure 7a shows the EDX line scan analysis made through the oxide nodule grown on the sample

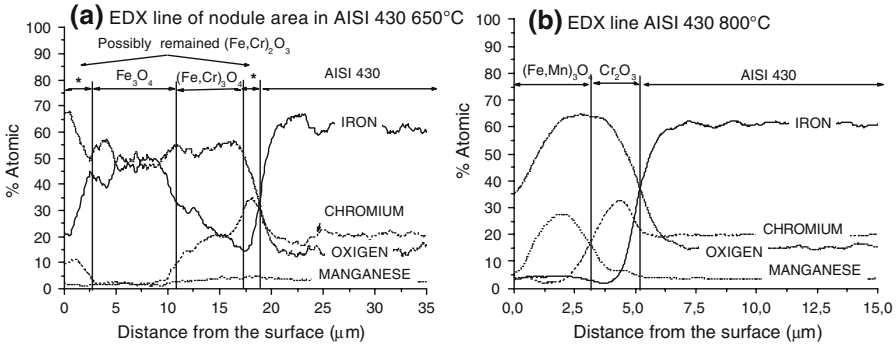

Fig. 7 EDX line scan analysis of AISI 430 ferritic stainless steel after steam oxidation up to 1000 h. **a** Nodule on the surface obtained at 650 °C and **b** sample surface at 800 °C

surface, which reveals that the nodule is formed by oxides of iron and chromium. Consonant with the XRD-GI results, the nodule is constituted of two phases, Fe_3O_4 and $(Fe,Cr)_3O_4$. Fe_3O_4 is placed at the outermost region, and $(Fe,Cr)_3O_4$ spinel is located below the magnetite. On the other hand, the thin scale that was grown on the substrate is mainly formed of $(Cr,Fe)_2O_3$, although the Cr_2O_3 and $(Fe,Mn)_3O_4$ identified by XRD-GI are also located in this thin scale. It can also observe the remained $(Fe,Cr)_2O_3$ in the outermost region and in contact with the substrate (areas with a concentration of Cr higher that that in the nodule).

On the other hand, the EDX scan line performed to the cross section of the AISI 430 sample oxidized at 800 °C is given in Fig. 7b, which shows the phases distribution in the layer the Cr_2O_3 is in contact with the substrate and $(Fe,Mn)_3O_4$ is located at the top of the chromia layer.

Discussion

Steam Oxidation of P-91 Ferritic-Martensitic Steel

As shown in the Section "Oxide scale characterization", the oxide scale that is formed on P-91 in a 100% steam atmosphere at 800 °C is bigger than the scale formed at lower temperature, 650 °C. On the other hand, the scale formed at 800 °C is composed by Fe_3O_4 and $(Fe,Cr)_3O_4$, although at 650 °C Fe_2O_3, hematite phase, is also formed on the surface.

At two temperatures, the outer scale formed is very porous, which could be associated with the formation of volatile species such as $Fe(OH)_{2(g)}$ by the reaction of the oxide scale with the vapour, as other authors as suggested, which assumes that the degradation of the Cr-rich oxide and the formation of non protective oxides is governed by the ratio $H_2O_{(g)}/O_2$ ratio and the $H_2O_{(g)}$ into the protective scale is the critical process leading to breakaway [6]. As experimental results illustrate, the formation of pores during the steam oxidation is higher at 800 than at 650 °C; this fact could be associated with a higher reactivity of the scale with the steam. With

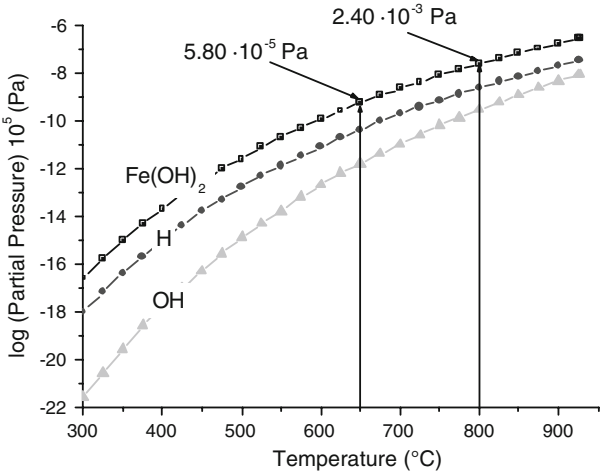

Fig. 8 Gaseous compounds that are formed in the thermodynamic equilibrium of a 90Fe/10Cr bulk and an atmosphere of 100% steam with the increasing of the temperature from 300 to 900 °C

the intention of evaluating the formation of volatile species during the steam exposure at high temperatures, a thermodynamic approximation was carried out with Thermo Calc. The calculations were performed considering a mixture of $Fe_{(s)}$ and $Cr_{(s)}$ with a 90Fe/10Cr relation and a H_2O/O_2 gas mixture, where the O_2 partial pressure is very low (less than 10^{-15} Pa), in order to simulate the experimental oxidation conditions. A temperature range of 300–900 °C and a pressure of 10^5 Pa were considered. Figure 8 shows the partial pressures of the gaseous species that are in thermodynamic equilibrium in the system composed of the 90Fe/10Cr theoretical alloy and the $H_2O/O_{2(g)}$ atmosphere (chemical species that are formed with a partial pressure higher than 10^{-17} Pa). It can be shown that at 650 °C the partial pressure of $Fe(OH)_2$ is two orders of magnitude lower than that at 800 °C, since the reactivity of the oxide scale with the steam is higher at 800 than that at 650 °C. On the other hand, this porosity in the magnetite can be also associated with the restriction of the transport of the Fe atoms in the inner layer [17].

The hematite is only observed in the oxidized samples at 650 °C, where is formed at the top of the scale. As said by other authors, the hematite formation is a consequence of a re-oxidation of the magnetite with the steam [20]. At 800 °C hematite phase is not formed since the formation of this phase is associated with moderate oxidation rates [13, 17].

The results show that the inner layer is composed by $(Fe,Cr)_3O_4$ spinel, in accordance with others authors [20, 21], although other works presented elsewhere showed that the inner scale formed is composed of a mixture of Fe_3O_4 and $(Fe,Cr)_3O_4$ [2, 6, 14].

With the aim of reproducing the oxidation conditions, thermodynamic approximations were carried out obtaining the main phases that are thermodynamically stables in the steam oxidation. Several thermodynamic simulations were carried out using bulk compositions from 92Fe/8Cr to 88Fe/12Cr (to simulate the composition

of P-91 ferritic-martensitic steel) at a steam atmosphere at 10^5 Pa and at a temperature range of 650–800 °C. The steam fraction in the atmosphere composed by a mixture of $H_2O/O_2/Ar$ was varied from 0 to 1.0. This fraction is defined as $n(H_2O)/[n(H_2O) + n(O_2) + n(Ar)]$ where n is the number of moles, $n(O_2)$ and n(Ar) are kept constant considering $n(O_2)$ very low (partial pressure less than 10^{-15} Pa), to reproduce the steam oxidation conditions.

Figures 9 and 10 show the diagrams obtained for the simulation, which collect only the thermodynamically stable oxidized solid phases, the gaseous phase has been omitted to clarify the diagram. When the steam fraction is lower than 30 vol.% approximately, the main solid oxidized phases are FeO and $(Fe,Cr)_3O_4$. But when

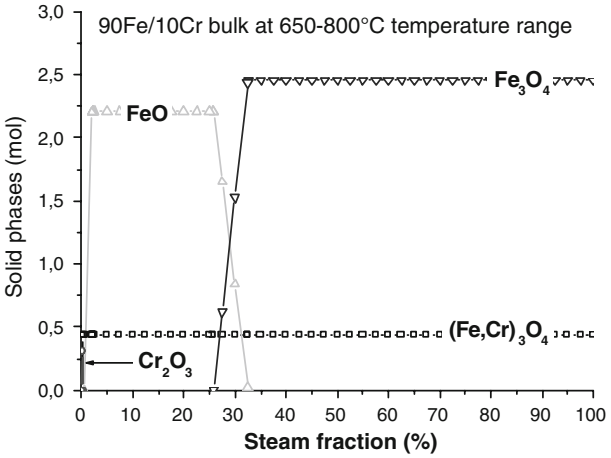

Fig. 9 Phases in thermodynamic equilibrium in a system composed by a 90Fe/10Cr bulk at 650–800 °C temperature range, increasing the steam fraction (vol.%)

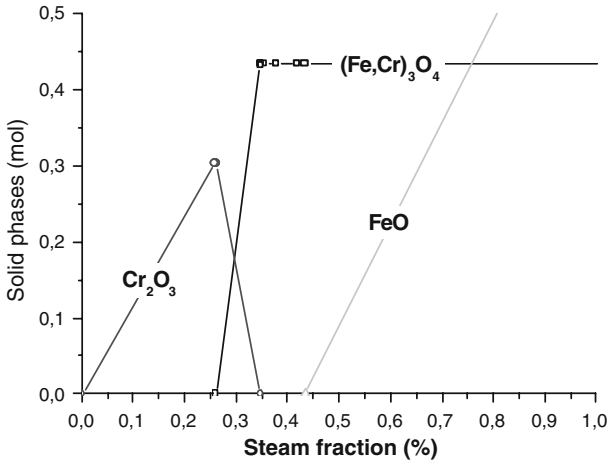

Fig. 10 Phases in equilibrium in a system composed by a 90Fe/10Cr bulk at 650–800° C temperature range, increasing the steam fraction (vol.%) up to 1.0 vol.%

the steam fraction is increased above than 30%, the solid phases in thermodynamic equilibrium are $(Fe,Cr)_3O_4$ and Fe_3O_4; the FeO becomes a non stable phase. Hematite is not a thermodynamic stable phase in all the range of steam fraction, although experimentally, was detected in the oxidation at 650 °C, when the oxidation rate was moderate.

Figure 10 is a magnification of the diagram of Fig. 9 and shows the phases in equilibrium when the steam fraction is lower than 1 vol.%. The Cr_2O_3 is the only stable phase when the steam fraction can be considered as a impurity, which is in agreement with other authors, which explain that the Cr_2O_3 phase is mainly formed on the surface of the 9–12% Cr ferritic-martensitic steels in dry air atmospheres at temperatures higher than 600 °C [3, 4], although in atmospheres composed by mixtures of water vapour and air the scales are formed of other less protective oxides than Cr_2O_3, such as Fe_3O_4 and $(Fe,Cr)_3O_4$ [1, 5, 6]; finally, other authors have reported that on Fe-13% Cr steel with dispersed yttria, at 700 °C, the scale in contact with the gas is mainly composed of $(Fe,Cr)_3O_4$ and at the temperature of 800 °C is composed of Cr_2O_3 [22].

In accord with the experimental results, the behaviour of the P-91 in steam oxidation at 800 °C can be considered as an accelerated test of the oxidation at 650 °C.

Steam Oxidation on AISI 430 Ferritic Stainless Steel

The oxidation rate of AISI 430 substrate at 650 °C is lower than that of the P-91. This is due to the formation of a layer on AISI 430 more protective than the scale obtained on P-91. The concentration of Cr in the AISI 430 is higher than in the P-91. Hence on the AISI 430 surface a layer mainly composed of $(Fe,Cr)_2O_3$ is formed which fails with the subsequent formation of nodules of Fe_3O_4 and $(Fe,Cr)_3O_4$.

Possibly, the degradation of the $(Fe,Cr)_2O_3$ is due to the vaporization of chromium from the oxide scale. Cr_2O_3 and $(Fe,Cr)_2O_3$ phases react with the water vapour and form volatile species such as $Cr_2OH_{(g)}$, $CrO_{3(g)}$ and $CrO_2(OH)_{2(g)}$ [1, 5, 15, 16] and with the chromium volatilization from the $(Fe,Cr)_2O_3$, Fe_2O_3 phase is formed [1], although as recently has been published the breakaway oxidation of ferritic steels in steam is related to a modification of transport processes in the substrates, due to hydrogen dissolution from the steam, promoting the internal oxidation of Cr rather than the formation of a protective scale, resulting in the formation of less protective Fe-rich oxides than chromia [23].

The steam oxidation behaviour of a steel with similar Cr content (18%Cr) has been studied elsewhere [11], and there the oxide scale formed on the steel, at 600 °C, is $(Fe,Cr)_2O_3$, although due to the chromium evaporation the protective oxide scale is transformed into non protective iron-rich oxide mainly composed by Fe_2O_3.

The ability of the AISI 430 ferritic stainless steel to preserve its protective properties in steam atmospheres is determined by the amount of chromium in the alloy and the chromium diffusion in the alloy, since the chromium content in the surface must be supplied from the alloy. This can be favoured by an appropriate control of the microstructure, the chromium supply to the surface is raised by

introducing an increased number of fast diffusion paths into the alloy, such as dislocations or grain boundaries [12, 22].

There are two different types of diffusion in the bulk of the alloy. The first is the atomic diffusion in the volume of the alloy, and the atomic mobility is the coefficient that describes it. The second is the grain boundary diffusion, which generally is greater than atomic diffusion in the bulk of the alloy. These two types of diffusion are thermally activated processes with an exponential dependence with the inverse of temperature. At 650 °C the diffusion (volume and grain boundary) of Cr atoms is relatively slow, and therefore the flux of Cr towards the oxide scale is not sufficient to remain the Cr_2O_3, since continuous degradation causes the loss of protection. In this case the scale transforms into a less protective phase than Cr_2O_3, the $(Fe,Cr)_2O_3$ oxide, witch is the main phase that was identified on the samples of AISI 430 after steam oxidation at 650 °C.

With the increasing of the temperature, the diffusion rate of Cr atoms also increases, and compensates the loss of Cr at the scale-gas interface. At 800 °C the growth of chromia scale is maintained by the supply of Cr atoms from the bulk of the steel. As an example, the Cr atomic motilities at 650 °C and 800 °C were obtained using the diffusion software DICTRA and MOB2 database. The coefficients of atomic motilities of Cr in a theoretical alloy composed of 84Fe/16Cr are $1.72\ 10^{-18}\ m^2 \cdot s^{-1}$ and $7.24\ 10^{-15}\ m^2 \cdot s^{-1}$ at 650 °C and 800 °C respectively. The Cr mobility at 800 °C is about four orders of magnitude than that Cr at 650 °C.

In agreement with the experimental results, the diffusion in volume and in the grain boundaries of Cr atoms at 650 °C are too low to allow the maintenance of the Cr_2O_3 protective layer, only a small amount of Cr_2O_3 has been detected by XRD-GI. On the other hand, at higher temperature, 800 °C the protective Cr_2O_3 can growth and be a protective scale as a result of the increase of the diffusion rate of Cr.

This increasing of the Cr diffusion rate at 800 °C produces two different phenomenon that make that the steam oxidation resistance of AISI 430 is higher at 800 °C than at 650 °C. Firstly, the mobility of Cr is enough to form a continuous layer of Cr_2O_3 on the substrate surface. On the other hand, although the Cr_2O_3 layer suffers the degradation of Cr by reaction with the steam, the flux of Cr atoms to the oxide scale compensate this loss of Cr, since the Cr diffusion rate is sufficiently high to remain the chromia scale.

In this case, the steam oxidation at 800 °C is not an accelerated test of the oxidation at 650 °C, since the oxidation rate at 800 °C is lower to that at 650 °C and also the phase composition is different.

Conclusions

During the long term oxidation of P-91 ferritic-martensitic steel at high temperatures, a bi-layered structure of Fe and Cr oxides is formed, which is thicker when the temperature is higher. At 650 °C the outer layer is composed of Fe_2O_3 and Fe_3O_4 and the inner of $(Fe,Cr)_3O_4$ spinel. On the other hand, at 800 °C no

significant amount of hematite is detected after 1000 h of steam exposure, only Fe_3O_4 and $(Fe,Cr)_3O_4$ are formed (the phases in thermodynamic equilibrium with a 100% steam atmosphere). Therefore, the steam oxidation test carried out at 800 °C can be considered an accelerated test for the steam oxidation at 650 °C.

The oxidation rate of AISI 430 in water vapour is lower than that of P-91, due to the higher concentration of Cr in the AISI 430. At 650 °C, a scale formed mainly by $(Fe,Cr)_2O_3$ is formed and also nodules of Fe and Cr oxides. At 800 °C the oxidation ratio is lower than at 650 °C, because at 800 °C a stable Cr_2O_3 scale is formed and remains along the time, because the diffusion of Cr compensates the loss of Cr by degradation of the Cr_2O_3. At 800 °C on AISI 430 the $(Fe,Mn)_3O_4$ spinel is also formed. In this case the oxidation at 800 °C is not considered as an accelerated test for the AISI 430 steam oxidation at 650 °C.

References

1. R. Peraldi and B. Pint, *Oxidation of Metals* **61**, 463 (2004).
2. P. J. Ennis and W. J. Quadakkers, *International Journal of Pressure Vessels and Piping.* **84**, 75 (2007).
3. A. P. Greeff, C. W. Louw, and H. C. Swart, *Surface and Interface Analysis* **30**, 120 (2000).
4. A. P. Greeff, C. W. Louw, and H. C. Swart, *Corrosion Science* **42**, 1725 (2000).
5. H. Asteman, K. Segerdahl, J. E. Svensson, L. G. Johansson, M. Halvarsson, and J. E., in Tang *High Temperature Corrosion and Protection of Materials 6, Prt 1 and 2, Proceedings* (2004), p. 775.
6. J. Ehlers, D. J. Young, E. J. Smaardijk, A. K. Tyagi, H. J. Penkalla, L. Singheiser, and W. J. Quadakkers, *Corrosion Science* **48**, 3428 (2006).
7. C. T. Fujii and R. A. Meussner, *Journal of the Electrochemical Society* **111**, 1215 (1964).
8. C. T. Fujii and R. A. Meussner, *Journal of the Electrochemical Society* **110**, 1195 (1963).
9. J. C. Vaillant, B. Vandenberghe, B. Hahn, H. Heuser, and C. Jochum, *International Journal of Pressure Vessels and Piping* **85**, 38 (2008).
10. Z. Yang, G.-G. Xia, M. S. Walker, C.-M. Wang, J. W. Stevenson, and P. Singh, *International Journal of Hydrogen Energy* **32**, 3770 (2007).
11. H. Asteman, J. Svensson, M. Norell, and L. Johansson, *Oxidation of Metals* **54**, 11 (2000).
12. X. Peng, J. Yan, Y. Zhou, and F. Wang, *Acta Materialia* **53**, 5079 (2005).
13. W. Quadakkers, P. J. Ennis, J. Ehlers, and T. Link, *VDI Berichte* **1484**, 113 (1999).
14. J. Zurek, E. Wessel, L. Niewolak, F. Schmitz, T.-U. Kern, L. Singheiser, and W. J. Quadakkers, *Corrosion Science* **46**, 2301 (2004).
15. S. Henry, A. Galerie, and L. Antoni, *Materials Science Forum* **369–3**, 353 (2001).
16. H. Asteman, J. Svenson, L. Johansson, and M. Norell, *Oxidation of Metals* **52**, 95 (1999).
17. P. J. Ennis and W. J. Quadakkers, *International Journal of Pressure Vessels and Piping* **84**, 82 (2007).
18. J. O. Andersson, T. Helander, L. Höglund, P. Shi, and B. Sundman, *Calphad* **26**, 273 (2002).
19. V. Lepingle, G. Louis, D. Allué, B. Lefebvre, and B. Vandenberghe, *Corrosion Science* **50**, 1011 (2008).
20. D. Laverde, T. Gomez-Acebo, and F. Castro, *Corrosion Science* **46**, 613 (2004).
21. Y. Chen, K. Sridharan, T. R. Allen, and S. Ukai, *Journal of Nuclear Materials* **359**, 50 (2006).
22. D. T. Hoelzer, B. A. Pint, and I. G. Wright, *Journal of Nuclear Materials* **283–287**, 1306 (2000).
23. E. Essuman, G. H. Meier, J. Zurek, M. Hänsel, and W. J. Quadakkers, *Oxidation of Metals* **69**, 143 (2008).